Nanodevices and Nanomaterials for Ecological Security

edited by

Yuri N. Shunin
Information Systems Management Institute
Riga, Latvia

and

Arnold E. Kiv
K.D. Ushinskiy South-Ukrainian National Pedagogical University
Odessa, Ukraine

Published in Cooperation with NATO Emerging Security Challenges Division

Proceedings of the NATO Advanced Research Workshop on
Nanodevices and Nanomaterials for Ecological Security
Riga, Latvia
20–23 June 2011

Library of Congress Control Number: 2012936661

ISBN 978-94-007-4121-8 (PB)
ISBN 978-94-007-4118-8 (HB)
ISBN 978-94-007-4119-5 (e-book)
DOI 10.1007/978-94-007-4119-5

Published by Springer,
P.O. Box 17, 3300 AA Dordrecht, The Netherlands.

www.springer.com

Printed on acid-free paper

Contents

Chapter 9
CNT Arrays Grown upon Catalytic Nickel Particles as Applied in the Nanoelectronic Devices: *Ab Initio* Simulation of Growth Mechanism

Yu.F. Zhukovskii, E.A. Kotomin, S. Piskunov, and S. Bellucci

Abstract Carbon nanotubes, due to their exceptional and unique properties, have aroused a lot of research interest making them promising candidates as interconnects for future high-speed nanoelectronics. To predict a growth mechanism for carbon nanotubes (CNTs) upon a metal particle as synthesized in the porous membrane block then incorporated in the nanoelectronic device, we have performed a series of large-scale DFT-LCAO calculations using the *CRYSTAL-06* code. Carbon adatoms can appear upon the densely-packed Ni(111) catalyst surface due to dissociation of hydrocarbon molecules (*e.g.*, CH_4) when applying the CVD method for the nanotube growth. We have started with adsorption properties of carbon atoms. Then, we have simulated the regular C/Ni(111) interface, where adatoms initially form a monolayer which can be disintegrated to nanoflakes gradually transforming into CNT embryos (in the form of semi-fullerenes) and, finally, into the capped CNTs ($d_{C-C} \approx 1.42$ Å) with either armchair or zigzag chirality. Periodicity of this system results in models of infinite arrays (bundles) of single-walled (SW) CNTs with a diameter 8.0–8.2 Å and the inter-tube distance 4.2–4.6 Å (depending on chirality). Analyzing the results of calculations on the CNT/Ni interconnect, we have observed a considerable transfer of the electronic

Yu.F. Zhukovskii (✉) • E.A. Kotomin
Institute of Solid State Physics, University of Latvia, 8 Kengaraga str., LV-1063 Riga, Latvia
e-mail: quantzh@latnet.lv

S. Piskunov
Institute of Solid State Physics, University of Latvia, 8 Kengaraga str., LV-1063 Riga, Latvia

Faculty of Computing, University of Latvia, 8 Kengaraga str., LV-1586 Riga, Latvia

Faculty of Physics and Mathematics, University of Latvia, 8 Kengaraga str., LV-1002 Riga, Latvia

S. Bellucci
INFN-Laboratori Nazionali di Frascati, Via Enrico Fermi 40, 00044 Frascati (Rome), Italy
e-mail: bellucci@lnf.infn.it

Y.N. Shunin and A.E. Kiv (eds.), *Nanodevices and Nanomaterials for Ecological Security*, NATO Science for Peace and Security Series B: Physics and Biophysics, DOI 10.1007/978-94-007-4119-5_9,

charge from the metallic catalyst towards the nanotube (up to ~1.4 *e per* contacting C atom) accompanying by substantial redistribution of the electronic density, especially in the case of nanostructured Ni(111) containing nickel nanoclusters. The nanostructured morphology of metal substrate has been found to be the most effective for the growth of CNT bundles.

Keywords Smooth and nanostructured Ni(111) substrates • Adsorption and dissociation of CH_4 molecule • Association of C adatoms • Swelling of carbon nanoflakes • Formation of carbon semi-fullerenes • Growth of capped CNTs • DFT-LCAO CRYSTAL code

9.1 Introduction

The continuous miniaturization of electronic devices, together with the high integration level and the increase of working frequencies and power density require the application of innovative chip interconnects and vias, to avoid a technological bottleneck with current Cu-interconnects in the near future [1] Traditional interconnect microtechnology will no longer satisfy future performance requirements: whereas critical dimensions of transistors are now far below 100 nm, the widths of Cu-interconnects are still on a micron scale, due to the high susceptibility of copper atoms to electromigration at high current densities. Unconventional interconnects and innovative materials are being studied as replacements for copper interconnects. Exceptional and unique electronic properties of carbon nanotubes (CNTs) [2] make them very promising candidates as interconnects for the future high-speed nanoelectronics. CNTs grown in the periodically distributed pores of insulated membranes [3] are found to be well-protected from external influence and ecologically safe, being important constituents of nanoelectronic devices. However, this application is still hindered by experimental inability to reproduce reliable growth of CNTs with predetermined chirality indices, since existing methods of nanotube synthesis yield a mixture of metallic and semiconducting nanotubes.

The growth of capped CNTs atop the particles of a metallic catalyst using the method of chemical vapor deposition (CVD) is believed to be the promising approach for gaining a control over the properties of nanotubes [4]. Moreover, the CVD growth of nanotubes can be achieved at low temperature, which is another important requirement for application of CNTs in nanoelectronics. The atomistic structure of interconnect between the nanoparticle of metallic catalyst and the CNT is important for understanding both the electronic transport through the nanotube and the mechanism of its growth. Decomposition of gas-phase carbon-hydrogen precursors (C_nH_m) on the catalyst surface is the first step for the CVD growth of CNTs. This is followed by the two important processes: (*i*) the diffusion of carbon atoms (a rate-determining step) either upon the catalyst particle surface or across its interior [5], and (*ii*) the nucleation of the graphitic fragment (carbon nanoflake) followed by further incorporation of carbon atoms into the growing nanotube,

which determines CNT chirality [6]. Depending on the size and structure of such a catalyst particle, either well-separated single-wall (SW) nanotubes, their bundles (containing up to several hundreds of the closely-packed nanotubes of different chiralities) or multi-wall (MW) nanotubes, whose shells also possess various chiralities, could be synthesized. The microscopic images of CNTs growing from the catalytic nanoparticles [7] help to model the Me-CNT junction. The optimal performance of carbon nanotubes requires a control of their structural properties [8], *e.g.*, size, length, chirality, which remains a significant difficulty for the widespread applications of CNTs in high-technology devices.

Synthesis of nanotubes mainly requires the presence of transition-metal element or alloy catalysts (*i.e.*, Co, Fe, Ni, Y, *etc.* [9]). Both SW and MW CNTs and their bundles have been synthesized *via* the interaction of metal catalyst nanoparticles with either carbon or hydrocarbon vapor at relatively high temperatures. These catalysts are crucial for the controlled synthesis of SW CNTs by means of CVD [10]. However, the exact role of metal atoms in the growth of SW CNTs is still unclear [11].

In the present paper, we discuss the results of systematic large-scale first-principles calculations on 2D periodic models of carbon-containing adsorbate upon both smooth and nanostructured Ni(111) substrate, varied from the CH_4 molecules up to the gradually growing bundles of capped SW CNTs possessing either *ac*- or *zz*-type chirality. The paper is organized as follows: Section 9.2 deals with the computational details. Models of different configurations for C/Ni interfaces as well as their properties are discussed and compared in Sect. 9.3, while Sect. 9.4 presents general conclusions.

9.2 Computational Details

The DFT-LCAO method (Linear Combination of Atomic Orbitals within the Density Functional Theory), as implemented in the *CRYSTAL-06* code [12], has been used to describe both 1D nanotubes and 2D sheets in their original space form, unlike the Plane-Wave (PW) methods, which are quite widespread in the study of low-dimensional periodic systems, including CNT-Me interconnects [13–15]. Indeed, to restore 3D periodicity in the PW nanotube calculations (necessary but artificial), the *x*-*y* supercell of nanotubes is introduced: the NTs are placed into a square array with the inter-tube distance equal to 1–3 nm. At such separations the NT-NT interaction is usually rather small, however, the convergence of results obtained in such PW calculations depends on the artificial inter-tube interactions, thus, additional computational efforts should be provided to ensure their negligibility. Analogous problems appear also in PW calculations on the 3D slab models (containing vacuum gaps). Such an artifact does not appear when using the LCAO formalism for simulation of nanotubes and slabs. Our latest calculations have been performed for a number of configurations of carbon-containing adsorbate above the Ni substrates.

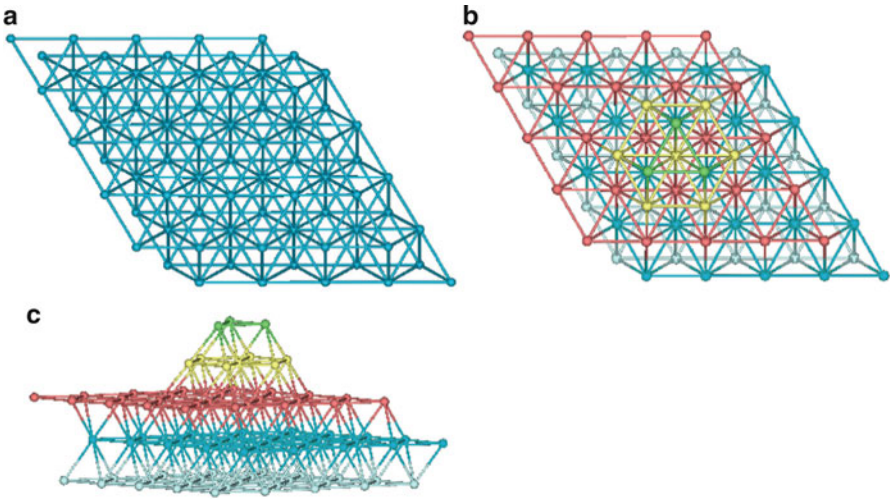

Fig. 9.1 Images of smooth Ni(111) 4 × 4 surface supercell (**a**) containing 10-atom Ni nanocluster upon the surface: atop (**b**) and aside (**c**) views. Each plane of nanostructured model is shown by a different color (*grayscale halftones*). The lower (*light-blue*) plane either coincides with the central layer of a 5-layer slab or it is one of surface planes in a 3-layer slab

The LCAO formalism was successfully applied earlier by us for simulations on smooth and nanostructured Ni(111) substrates [16] as well as on SW nanotubes obtained from AlN [17], BN [18] and TiO_2 [19]. The all-valence basis sets (BSs) of atomic GTFs are used as described elsewhere: Ni (8*s*–64111*sp*–41*d*) [16], and O (8*s*–411*sp*–1*d*) [18] which have been slightly re-optimized for valence and virtual shells. Analogously, the C (6*s*–311*sp*–11*d*) BS [12] has been re-optimized too. The exchange-correlation DFT functional by Perdew, Burke and Ernzerhof (PBE) within the Generalized Gradient Approximation (GGA) [20] has been used in our spin-polarized calculations. To provide a balanced summation in both direct and reciprocal lattices, the reciprocal space integration has been performed by sampling the Brillouin zone with the 2 × 2 × 1 Pack-Monkhorst mesh [21] which results in 2 *k*-points in total for 5 × 5 surface supercell of Ni(111) slab models (Fig. 9.1). Calculations are considered as converged when the total energy differs by less than 10^{-7} a.u. in the two successive cycles of the self-consistency procedure. Smearing temperature of 0.001 a.u. applied to the Fermi function has been chosen for relatively low temperature, to exclude the appearance of the artificially enhanced magnetic moment. Total geometry optimization has been performed in all our calculations.

9.3 Results and Discussion

Let us compare and verify the results of *ab initio* simulations performed on 2D periodic models describing peculiarities of the initial stage of growth for the bundle of SW CNTs upon the catalyst particle. The only limitation of such a 2D model is

that both the chirality and diameter of CNTs in the bundle are equivalent. This is a first attempt to simulate the periodic distribution of carbon nanotubes grown upon the catalyst surface in the framework of 2D periodic model.

9.3.1 Pure Ni Substrate

We consider 2D adsorbate-free models of both smooth and nanostructured Ni(111) surfaces (Fig. 9.1) as the first stage for these simulations,. The supercell (SC) of smooth nickel (111) slab shown in Fig. 9.1a has been constructed from cubic *fcc* Ni crystal (space group *Fm3m*, the lattice constant 3.532 Å, $\alpha = \beta = \gamma = 90°$) and a 5-layer slab containing 125 atoms *per* SC. The nanostructured Ni(111) surface contains a cluster *per* 5 × 5 supercell atop the smooth (111) surface (Fig. 9.1b, c) which includes seven and three nickel atoms in the corresponding sites of the first and second (111) sublayers, respectively. Properties of smooth and nanostructured Ni(111) surfaces were analyzed in our previous paper [16].

9.3.2 Model of Hydrocarbon Molecule Dissociation upon Ni Substrates

When using the CVD method [4], the appearance of the network from the adsorbed carbon atoms, which can be gradually transformed to CNT structures, follows by dissociation of hydrocarbon molecules, *e.g.*, simplest CH_4 (point group T_d, equilibrium length of C–H bond is 1.086 Å [22]), flowing towards the substrate. We estimate the dissociation energies for CH_4 molecules (E_{diss}) atop both substrates (see Fig. 9.2 for details) according to the total energy balance of the two-step dissociation mechanism:

$$(CH_4)_{ads} \rightarrow (CH)_{ads} + 3H_{ads}, \tag{9.1a}$$

$$(CH)_{ads} \rightarrow C_{ads} + H_{ads}. \tag{9.1b}$$

Energetically the most preferable site for adsorption of the methane molecule atop the Ni substrate has been found to be the hollow *fcc* site, due to orientation compatibility between CH_4 molecule and both smooth and nanostructured Ni(111) surface (Fig. 9.2). Recent simulations on methane dissociation and adsorption on smooth Ni(111), Pt(111), Ni(100) and Pt(100) as well as on slightly reconstructed Pt(110)–(1 × 2) surfaces [23] have indicated the energetic preference for CH_4 molecule and CH_3 radical to be adsorbed upon the atop site and the hollow *fcc* site of Ni(111) substrate, respectively. However, in those simulations, an alternative mechanism of dissociation has been considered:

$$(CH_4)_{ads} \rightarrow (CH_3)_{ads} + H_{ads}, \tag{9.2a}$$

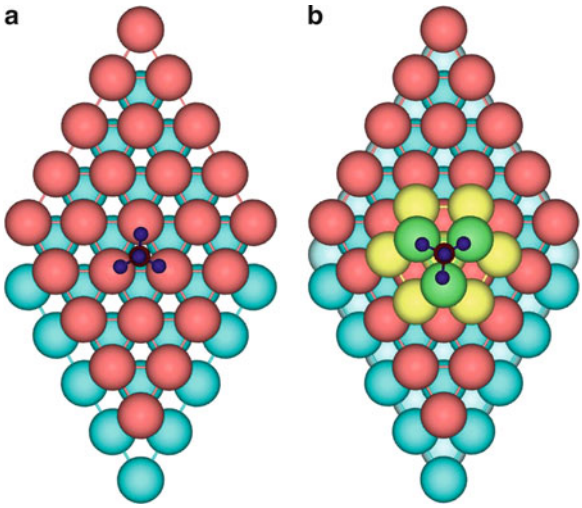

Fig. 9.2 Schematic models of CH_4 molecule dissociation upon both smooth (**a**) and nanostructured (**b**) Ni(111) substrate

$$(CH_3)_{ads} \rightarrow C_{ads} + 3H_{ads}. \tag{9.2b}$$

Obviously, Eqs. 9.1a and 9.2b look similar according to the symmetry of dissociation path. We have used the former, to avoid extremely time-consuming calculations for obtaining qualitatively close results.

The calculated values of initial binding energy (E_{ads}) *per* CH_4 molecule upon the adsorption sites shown in Fig. 9.2 have been estimated to be ~1.0 eV (for both smooth and nanostructured Ni substrate). The comparison of the total dissociation energies of CH_4 molecule upon the same sites clearly shows that the presence of small periodically distributed polyhedral nanoclusters (Fig. 9.2b) results in preferable carbon atomization. The calculated energies of a complete dissociation (E_{diss}) have been found to be 2.33 eV and 2.17 eV *vs.* 4.87 eV, respectively. It clearly indicates that the presence of edges upon the Ni particle relieves carbon atom association and further CNT growth. Detailed analysis of possibilities for CNT growth can be performed based on association of carbon adatoms released after complete dissociation of hydrocarbon molecules upon the nickel substrate.

9.3.3 *Models of Single C Atom Adsorption upon Ni*

The binding energies of the newly-formed C_{ads} adatoms, both single and associated, atop the smooth and nanostructured Ni(111) surfaces have been calculated using the following equation:

$$E_{bind} = -\left(E_{complex} - E_{slab} - n_C E_C\right)/n_C, \tag{9.3}$$

where $E_{complex}$ is the calculated total energy of the slab with the attached C_n adsorbate, E_{slab} is the total energy of the bare slab, $E_{C\ is}$ the energy of a single

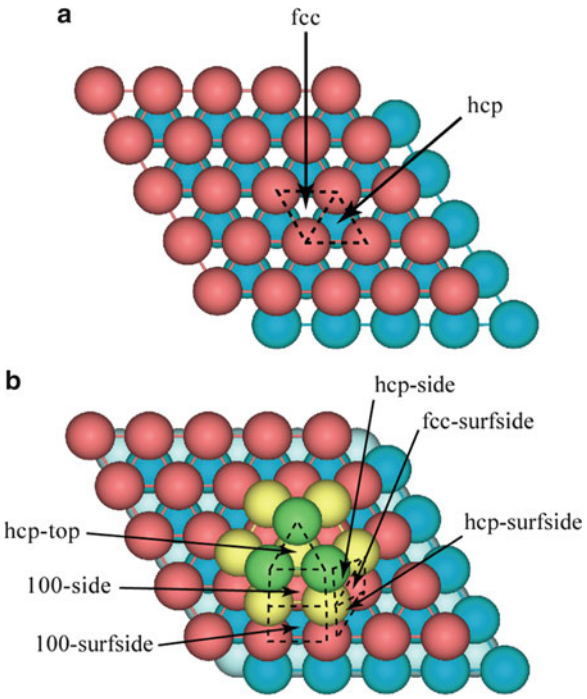

Fig. 9.3 Models of single C atom adsorption molecule upon both smooth (**a**) and nanostructured (**b**) Ni(111) substrates

carbon atom in its ground state, and n_C is a number of carbon atoms *per* supercell. The corresponding models are shown in Fig. 9.3a, b.

Using Eq. 9.3 we have estimated the binding energies of carbon atoms upon different substrates and have drawn the conclusions on their ability to form carbon nanotubes (Table 9.1). It is important that C atoms being adsorbed upon the network of *fcc* and *hcp* hollow sites upon the Ni(111) surface (the former are energetically slightly less favorable for adsorption as compared to the former) result in the appearance of almost an ideal graphene monolayer since its misfit with a nickel substrate is almost neglecting. Our calculations do not confirm energetic preference for penetration of C_{ads} atoms into the substrate as observed recently in models of the C/Cu(111) interface [5]. Energetically the most stable adsorption positions for the carbon atom with E_{bind} of ~8 eV have been found to be aside (100) sites at the nanostructured Ni(111) surface. We predict the increase of catalytic activity of nanostructured Ni(111) surface due to the nanofacet formation that potentially can play a role in the predictable growth of CNT.

9.3.4 Models of Association of C Atoms upon Ni Substrates

After modeling adsorption of single C atoms, we have considered their further association. In our model of regular adsorption of carbon atoms atop the most

Table 9.1 Calculated binding energies *per* single carbon adatom upon smooth and nanostructured Ni(111) catalyst (Fig. 9.3a, b)

Structure	E_{bind} (eV)
hcp-Ni(111)	7.09
fcc-Ni(111)	6.39
hcp-top-nano-Ni(111)	7.13
001-side-nano-Ni(111)	8.08
001-surfside-nano-Ni(111)	7.19
hcp-side-nano-Ni(111)	6.93
fcc-surfside-nano-Ni(111)	7.19
hcp-surfside-nano-Ni(111)	7.48

preferable *hcp* sites upon a smooth Ni(111) surface (Table 9.1), E_{bind} *per* C atom has been found to be 5.48 eV, *i.e.*, noticeably smaller than E_{bind} for a single adatom atop the same site (7.09 eV) (*vs.* experimental value of 6.9 eV [24]). This difference could be caused by a strong lateral interaction between adatoms. Translation vector for such a regular C adsorbate structure has a length of 2.47 Å which is structurally compatible with the (111) face of adsorbent (length of analogous vector on nickel substrate is 2.49 Å), *i.e.*, their mismatch is only ~0.8%. To form the quasi-graphene structure, the neighboring carbon adatoms can be positioned above the neighboring *fcc*- and *hcp*-adsorption sites (Fig. 9.3a), *i.e.*, packing of adatoms must be twice larger than in the case of regular adsorption upon the same type of surface sites. To form semi-fullerene-like embryos from quasi-graphene islands upon the surface of nickel catalyst, they must contain pentagons, which result in swelling of the flakes with a further growth of fullerene-like structures [25]. We considered this process atop a smooth Ni(111) substrate by gradually increasing the number of C adatoms (Fig. 9.4):

The binding energies compared in Fig. 9.4a, b clearly show that an initial formation of hexagonal C-rings is more preferable than pentagons. At the same time, a gradual growth of a quasi-graphene flake and its further swelling, due to the appearance of aside pentagons (Fig. 9.5f), make the binding energies of semi-fullerenes, containing carbon pentagon or hexagon in the center, more close. After achieving a certain critical diameter of semi-fullerene embryo, the further growth continues as CNT growth [11, 26]. In the case of a smooth Ni(111) substrate, the critical diameter is ~0.8–0.9 nm. Figure 9.4e, f show the appearance of capped CNTs with *zz*- and *ac*-chiralities, respectively. Since the number of C atoms directly contacting with the substrate are limited by the circles in the latter configurations, their E_{bind} values decrease noticeably. Since we have used 2D periodic models of CNT-Ni interconnects, they describe the growth of SW CNT bundles containing nanotubes of identical chiralities rather individual CNTs. Parameters of CNT bundles containing nanotubes of either *ac*- or *zz*-chiralities are comparable with those measured experimentally or simulated theoretically [4].

Obviously, the appearance of carbon pentagons upon a smooth nickel (111) substrate demands a certain energy supply. On the other hand, the presence of Ni nanoclusters (Fig. 9.5) as well as other structural defects on a smooth substrate makes the growth of graphene monolayer unlikely, since the curvature of carbon adlayer clearly indicates the presence of both hexagons and pentagons from

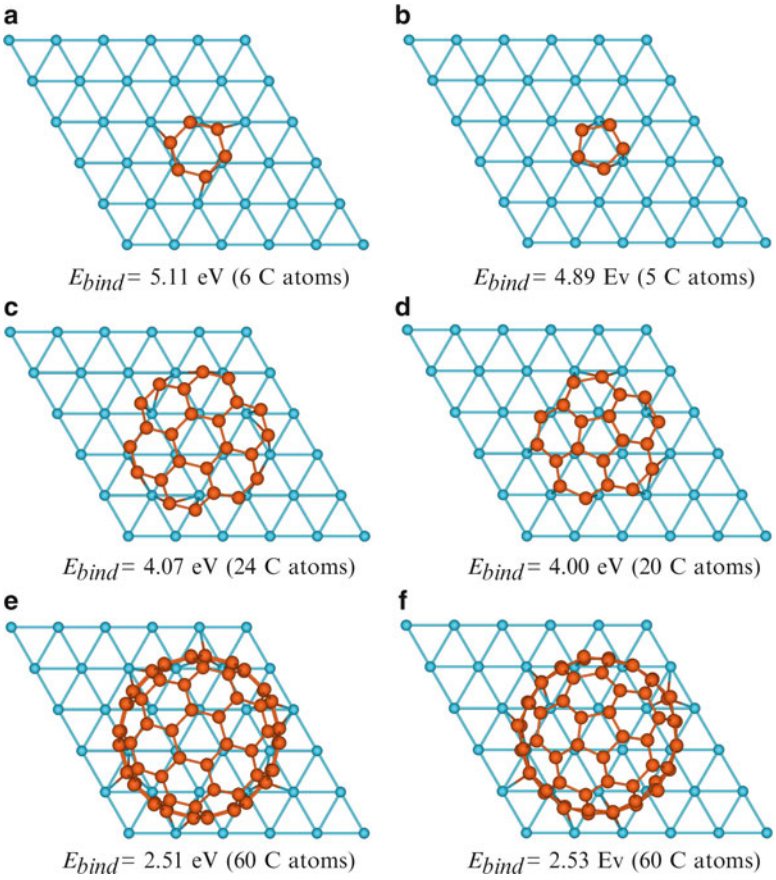

Fig. 9.4 Models of carbon semi-fullerene embryos growth upon 5 × 5 surface supercell of smooth Ni(111) slab, beginning with appearance of C-ring islands (**a**, **b**), their growth to quasi-graphene swelled flakes (**c**, **d**), up to creation of capped nanotubes with: armchair- (**e**) and zigzag-type (**f**) chiralities

C atoms. Thus, the nanostructured Ni(111) substrate is a good catalyst for the growth of both capped carbon nanotubes and fullerenes. The calculated bonding energies between CNTs growing on smooth and nanostructured Ni substrates differ substantially, thus, confirming noticeably larger stability of the latter CNT-Ni contacts.

9.3.5 Electronic Structure of SW CNTS Grown on Ni Substrates

Substantial electronic charge transfer and redistribution of the electronic density inside the SW CNT-Ni interconnect is caused by a strong chemical bonding. The magnitudes of charge transfer towards the nearest C atoms across the interfaces or

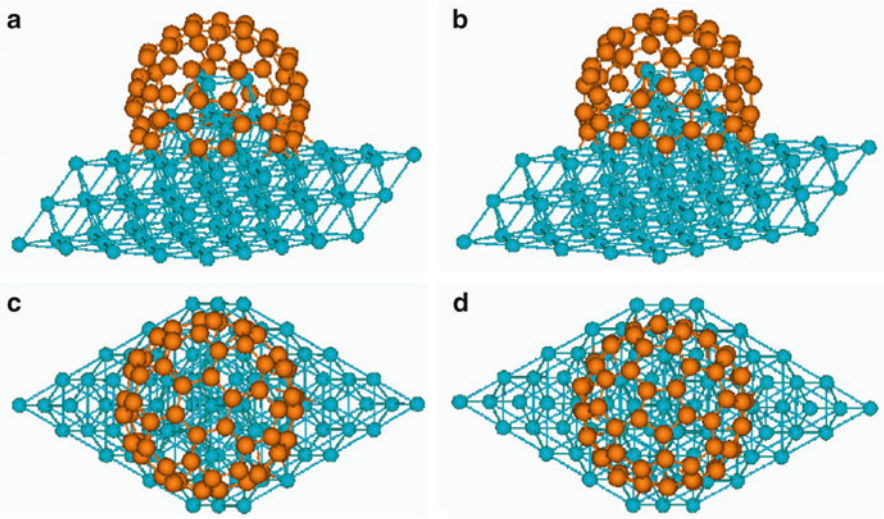

Fig. 9.5 Aside (*upper*) and atop (*lower*) views of 2D 4 × 4 supercells containing CNT of either *ac*- (**a**) or *zz*-(**b**) type chirality upon the nanostructured Ni(111) surface

Table 9.2 Calculated charge, Δq (in e), transferred from to C structures positioned atop Ni

C/Ni(111) structure (with number of contacting carbon atoms)	Charge transfer to all C atoms contacted to Ni	Δq *per* C atom
zz-CNT atop smooth Ni(111) (10)	13.84	1.38
ac-CNT atop smooth Ni(111) (12)	14.07	1.17
ac-CNT atop nanostructured Ni(111) (12)	13.34	1.11
zz-CNT atop nanostructured Ni(111) (10)	10.14	1.01
Single C atop *hcp* site upon Ni(111) (1)	0.97	0.97
C atoms atop *hcp*-sites upon Ni(111) (25)	23.75	0.95
C atoms forming embryo atop Ni(111) (6)	3.93	0.65
Graphene (0001) sheet atop Ni(111) (50)	28.00	0.56

interconnects are presented in Table 9.2. In the case of interconnects between the *ac*-CNT bundle and smooth Ni(111) substrate, the interfacial C ring accepts the electronic charge of 14.07 e (by 12C atoms). For *zz*-CNT/Ni(111) in the same model the Ni substrate transfers the electronic charge of 13.84 e (10C atoms) to the contacting nanotube ring.

The comparison of electron charge redistributions in SW CNT of the same chirality grown from both smooth and nanostructured Ni substrates (Figs. 9.6 and 9.7, respectively) shows the essential difference which can be described by a substantial influence of Ni nanocluster positioned upon the substrate (Fig. 9.1c). The two important differences are: (*i*) noticeably larger difference of densities for planes crossing boundary carbon rings, and (*ii*) whereas carbon rings above the Ni-CNT interconnect in the case of smooth substrate are characterized by the

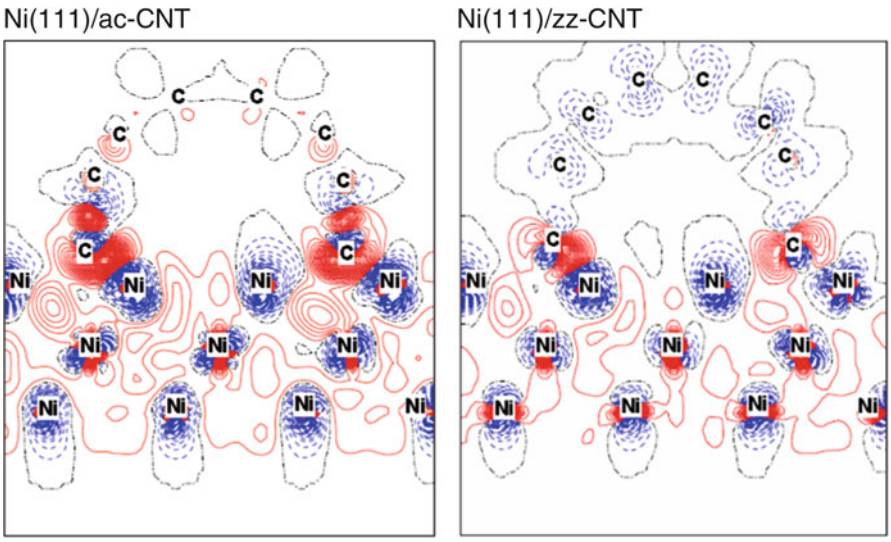

Fig. 9.6 Charge redistributions between the bundles of *ac*-CNT (*left plot*) and *zz*-CNT (*right plot*) with the smooth Ni(111) substrate (the total density in the SW CNT-Ni interconnect minus the sum of electronic densities in separate SW CNT and nickel substrate). *Black* (*dash-dot*) *isolines* correspond to the zero level. *Blue* (*dash*) *isolines* stand for the decrease in the electron density while *red* (*solid*) *lines* for the increase. Isodensity curves are drawn from −0.05 to +0.05 e a.u.$^{-3}$ with the increment of 0.00167 e a.u.$^{-3}$

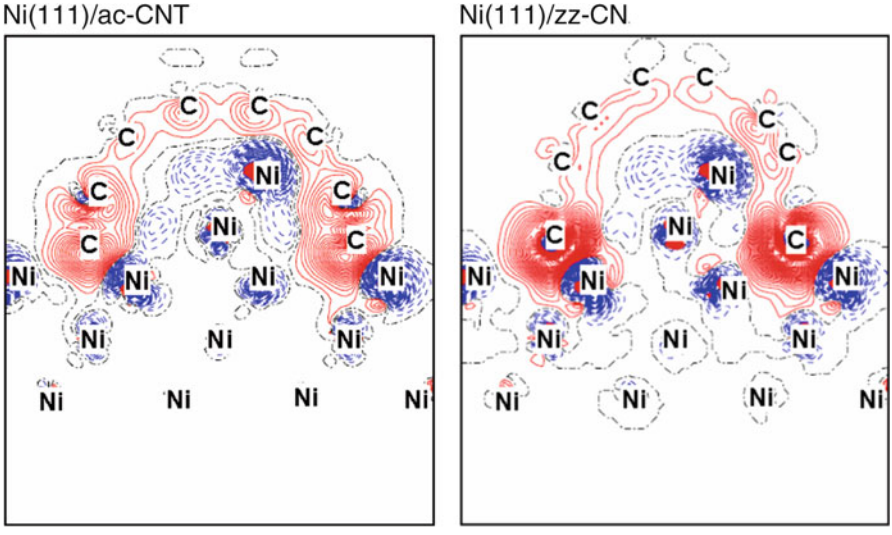

Fig. 9.7 Charge re-distributions between the bundles of *ac*-CNT (*left plot*) and *zz*-CNT (*right plot*) with the nanostructured Ni(111) substrate. Details of plots are the same as in Fig. 9.6

deficiency of electron density (especially in *zz*-CNT), all the carbon rings above the nanostructured substrate possess the *enhanced* electronic density, particularly, supplied by a Ni nanocluster.

As a result, the Mulliken charges of the boundary carbon atoms above a smooth substrate are slightly larger than those above a nanocluster (Table 9.2), which can be explained by a particular electronic charge transfer from the higher carbon rings to the interconnect. On the contrary, the markedly higher values of E_{bind} for the nanostructured Ni-CNT interconnects (as compared in Fig. 9.5) can be explained by a considerably higher electronic density redistribution in them, *i.e.* the interconnect bonding is found to be much more strong.

9.4 Conclusions

We have presented the 2D models of CNT bundle growth upon both smooth and nanostructured Ni(111) catalyst substrates. For these simulations, a series of large-scale DFT-LCAO calculations have been performed using the *CRYSTAL-06* computational code. The obtained results of the first-principles calculations predict a quite effective and reproducible mechanism for the growth of capped carbon nanotubes upon the nanostructured Ni(111) substrate. The driving force of CNT growth upon the catalyst surface (using CVD method providing a permanent flow of hydrocarbon molecules towards the substrate) is the formation of C-pentagons inside the graphene flakes, which gradually swell forming quasi-fullerene embryos upon the surface. They appear as a result of dissociation of hydrocarbon molecules moving towards the catalyst substrate.

The formation of C-pentagons inside the graphene monolayer upon the smooth catalytic substrate island demands a certain energy supply, in contrast to a nanostructured nickel (111) substrate, where the growth of C_n flakes with a mixed hexagon-pentagon morphology occurs spontaneously and results in the formation of the capped nanotubes firmly connected to the nanoclusters grown upon the Ni (111) substrate. The calculations on the electronic properties of CNTs grown upon the Ni substrate confirm the decisive role of Ni nanoclusters in strengthening the Ni-CNT interconnects. The analysis of these properties has allowed us to clarify the reason for noticeable differences between the *ac*- and *zz*-CNTs.

At the atomistic, lowest level of the multi-scale modeling, *ab initio* methods can be used for determining the electronic structure of the assumed carbon-metal nanocomposites and for the better understanding of physical properties in nanoelectronic devices containing CNT-Me interconnects. The obtained results could also be applied for constructing single-particle Hamiltonian used in the analytical tight-binding calculations of the conducting channels in the Me/MW-CNT interconnects, as well as in further molecular dynamics and kinetic Monte-Carlo simulations.

Acknowledgments This study has been partly supported by EC FP7 CATHERINE Project. S.P. is thankful for the financial support through the ESF project Nr. 2009/0216/1DP/1.1.1.2.0/09/APIA/VIAA/044. Authors are grateful to Prof. R.A. Evarestov for stimulating discussions.

References

1. Murarka SM, Verner IV, Gitmann RJ (2000) Copper – fundamental mechanisms for microelectronic applications. Wiley, New York
2. Ahlskog M, Laurent Ch, Baxendale M, Huhtala M (2004) Electronic properties and applications of carbon nanotubes. In: Nalwa HS (ed) Encyclopedia of nanoscience and nanotechnology, vol 3. American Science, Los Angeles, pp 139–161
3. Ciambelli P, Sannino D, Sarno M, Fonseca A, Nagy JB (2004) Hydrocarbon decomposition in alumina membrane: an effective way to produce carbon nanotubes bundles. J Nanosci Nanotechnol 4:779–787
4. Loiseau A, Gavillet J, Ducastelle F, Thibault J, Ste´phan O, Bernier P (2003) Nucleation and growth of SWNT: TEM studies of the role of the catalyst. C R Phys 4:975–991
5. Chen H, Zhu W, Zhang Z (2010) Contrasting behavior of carbon nucleation in the initial stages of graphene epitaxial growth on stepped metal surfaces. Phys Rev Lett 104:186101 (1–4)
6. Zhu H, Suenaga K, Hashimoto A, Urita K, Hata K, Iijima S (2005) Atomic-resolution imaging of the nucleation points of single-walled carbon nanotubes. Small 1:1180–1183
7. Hofmann S, Sharma R, Ducati C, Du G, Mattevi C, Cepek C, Cantoro M, Pisana S, Parvez A, Cervantes-Sodi F, Ferrari AC, Dunin-Borkowski R, Lizzit S, Petaccia L, Goldoni A, Robertson J (2007) In situ observations of catalyst dynamics during surface-bound carbon nanotube nucleation. Nano Lett 7:602–608
8. Amara H, Roussel J-M, Bichara C, Gaspard J-P, Ducastelle F (2009) Tight-binding potential for atomistic simulations of carbon interacting with transition metals: application to the Ni-C system. Phys Rev B 79:014109 (1–17)
9. Gavillet J, Thibault J, Stephan O, Amara H, Loiseau A, Bichara C, Gaspard J-P, Ducastelle F (2004) Nucleation and growth of single wall nanotubes: the role of metallic catalyst. J Nanosci Nanotechnol 4:346–359
10. Lin M, Pei Ying Tan J, Boothroyd C, Loh KP, Tok ES, Foo Y-L (2006) Direct observation of single-walled carbon nanotube growth at the atomistic scale. Nano Lett 6:449–452
11. Amara H, Bichara C, Ducastelle F (2008) Understanding the nucleation mechanisms of carbon nanotubes in catalytic chemical vapor deposition. Phys Rev Lett 100:056105 (1–4)
12. Dovesi R, Saunders VR, Roetti C, Orlando R, Zicovich-Wilson CM, Pascale F, Civalleri B, Doll K, Harrison NM, Bush IJ, D'Arco Ph, Llunell M (2006) CRYSTAL06 user's manual. University of Torino, Turin. http://www.crystal.unito.it/
13. Ding F, Larsson P, Larsson JA, Ahuja R, Duan H, Rose´n A, Bolton K (2008) The importance of strong carbon-metal adhesion for catalytic nucleation of single-walled carbon nanotubes. Nano Lett 8:463–468
14. Yazyev OV, Pasquarello A (2008) Effect of metal elements in catalytic growth of carbon nanotubes. Phys Rev Lett 100:156102 (1–4)
15. Börjesson A, Zhu W, Amara H, Bichara C, Bolton K (2009) Computational studies of metal-carbon nanotube interfaces for regrowth and electronic transport. Nano Lett 9:1117–1120
16. Piskunov S, Zvejnieks G, Zhukovskii YuF, Bellucci S (2011) Atomic and electronic structure of both perfect and nanostructured Ni(111) surfaces: first-principles calculations. Thin Solid Films 519:3745–3751
17. Zhukovskii YuF, Pugno N, Popov AI, Balasubramanian C, Bellucci S (2007) Influence of F centres on structural and electronic properties of AlN single-walled nanotubes. J Phys Condens Matter 19:395021 (1–18)

18. Zhukovskii YuF, Bellucci S, Piskunov S, Trinkler L, Berzina B (2009) Atomic and electronic structure of single-walled BN nanotubes containing N vacancies as well as C and O substitutes of N atoms. Eur Phys J B 67:519–525
19. Evarestov RA, Bandura AV, Losev MV, Piskunov S, Zhukovskii YuF (2010) Titania nanotubes modeled from 3- and 6-layered (101) anatase sheets: line group symmetry and comparative ab initio LCAO calculations. Physica E 43:266–278
20. Perdew JP, Burke K, Ernzerhof M (1996) Generalized gradient approximation made simple. Phys Rev Lett 77:3865–3868
21. Monkhorst HJ, Pack JD (1976) Special points for Brillouin-zone integrations. Phys Rev B 13:5188–5192
22. Duchovic RI, Hase WL, Schlegel HB, Frisch MJ, Raghavachari K (1982) Ab initio potential energy curve for CH bond dissociation in methane. Chem Phys Lett 89:120–125
23. Nave S, Tiwari AK, Jackson B (2010) Methane dissociation and adsorption on Ni(111), Pt(111), Ni(100), Pt(100), and Pt(110)-(1×2): energetic study. J Chem Phys 132:054705 (1–12)
24. Kalibaeva G, Vuilleumier R, Meloni S, Alavi A, Ciccotti G, Rosei R (2006) Ab initio simulation of carbon clustering on an Ni(111) surface: a model of the poisoning of nickel-based catalysts. J Phys Chem B 110:3638–3646
25. Fujita M, Saito R, Dresselhaus G, Dresselhaus MS (1992) Formation of general fullerenes by their projection on a honeycomb lattice. Phys Rev B 45:13834–13836
26. Alekseev NI, Charykov NA (2008) Nucleation of carbon nanotubes and their bundles at the surface of catalytic melt. Russ J Phys Chem A 82:2191–2201